Since January 2020 Elsevier has created a COVID-19 resource centre with free information in English and Mandarin on the novel coronavirus COVID-19. The COVID-19 resource centre is hosted on Elsevier Connect, the company's public news and information website.

Building and Environment 219 (2022) 109232

Contents lists available at ScienceDirect

Building and Environment

journal homepage: www.elsevier.com/locate/buildenv

A novel CO_2-based demand-controlled ventilation strategy to limit the spread of COVID-19 in the indoor environment

Bingxu Li [a,b], Wenjian Cai [a,*]

[a] School of Electrical and Electronic Engineering, Nanyang Technological University, 50 Nanyang Avenue, 639798, Singapore
[b] Energy Research Institute @ NTU (ERI@N), Interdisciplinary Graduate Programme, Nanyang Technological University, Singapore

ARTICLE INFO

Keywords:
Demand-controlled ventilation
COVID-19
CO_2 concentration
Event reproduction number
Ventilation control scheme

ABSTRACT

Ventilation is of critical importance to containing COVID-19 contagion in indoor environments. Keeping the ventilation rate at high level is recommended by many guidelines to dilute virus-laden respiratory particles and mitigate airborne transmission risk. However, high ventilation rate will cause high energy use. Demand-controlled ventilation is a promising technology option for controlling indoor air quality in an energy-efficient manner. This paper proposes a novel CO_2-based demand-controlled ventilation strategy to limit the spread of COVID-19 in indoor environments. First, the quantitative relationship is established between COVID-19 infection risk and average CO_2 level. Then, a sufficient condition is proposed to ensure COVID-19 event reproduction number is less than 1 under a conservative consideration of the number of infectors. Finally, a ventilation control scheme is designed to make sure the above condition can be satisfied. Case studies of different indoor environments have been conducted on a testbed of a real ventilation system to validate the effectiveness of the proposed strategy. Results show that the proposed strategy can efficiently maintain the reproduction number less than 1 to limit COVID-19 contagion while saving about 30%–50% of energy compared with the fixed ventilation scheme. The proposed strategy offers more practical values compared with existing studies: it is applicable to scenarios where there are multiple infectors, and the number of infectors varies with time; it only requires CO_2 sensors and does not require occupancy detection sensors. Since CO_2 sensors are very mature and low-cost, the proposed strategy is suitable for mass deployment in most existing ventilation systems.

1. Introduction

COVID-19 is a contagious respiratory disease caused by the novel SARS-CoV-2 virus [1]. Until Feb 11, 2022, COVID-19 pandemic has caused 404,910,528 infected cases including 5,783,776 deaths worldwide [2]. Many countries are currently experiencing a huge wave of infection with the new variant of SARS-CoV-2 called Omicron [3], which is proven to be much more transmissible than the previous strains [4–6] and can reduce vaccine efficacy [7–9]. The surge of COVID-19 infection cases puts considerable pressure on health systems and societies. Evidence shows that COVID-19 will continue and last for a long period [10,11]. Thus, developing efficient control strategies to prevent virus transmission and mitigate the infection risk is still essential at the present stage.

Modes of COVID-19 transmission include contact transmission, airborne transmission, and fomite transmission [12]. Contact transmission occurs when a person is in close contact with the infector; respiratory droplets containing virus reach the eyes, mouth and nose of a susceptible person and then cause infection. Airborne transmission occurs when a person inhales infectious droplet nuclei (aerosols) suspended in the air. Fomite transmission happens when a person touches surfaces contaminated by virus and then touches eyes, mouth, and nose [12]. Contact and airborne transmission are considered dominant transmission modes while fomite transmission is not [12].

Ventilation is important in limiting airborne transmission of COVID-19 in indoor environments [13]. Through the ventilation, outdoor fresh air is intentionally introduced into the space to dilute and replace infectious aerosols. Demand-controlled ventilation (DCV) is a widely-used ventilation framework which can achieve energy-efficient control of indoor air quality (IAQ) [14–16]. Under the DCV framework, the ventilation rate is dynamically adjusted according to the actual ventilation demand. That is, the ventilation is enhanced during the periods of high demand and reduced to conserve energy during the periods of low demand.

In the context of controlling COVID-19 transmission risk in indoor

* Corresponding author.
E-mail address: ewjcai@ntu.edu.sg (W. Cai).

https://doi.org/10.1016/j.buildenv.2022.109232
Received 26 February 2022; Received in revised form 3 May 2022; Accepted 23 May 2022
Available online 26 May 2022

Nomenclature

C	Indoor CO_2 concentration (unit:ppm)
C_{avg}	Average indoor CO_2 concentration (unit:ppm)
C_{ub}	Upper bound for the average indoor CO_2 concentration (unit:ppm)
C_{out}	CO_2 concentration of outside air (unit:ppm)
d	Deviation ratio
D	Dose of virus quanta inhaled by the susceptible person (unit:quanta)
E	Power consumption of the ventilation system (unit:W)
ER_q	Average virus quanta emission rate by each infector (unit: quanta/h)
I	The number of infectors
k	Virus deposition rate onto surfaces (unit:1/h)
n	Indoor virus quanta concentration (unit:quanta/m^3)
N	The number of occupants
p	Infection probability (risk) of the susceptible person
q	Outdoor ventilation rate (unit:m^3/h)
q_{lb}	Lower bound for the outdoor ventilation rate (unit:m^3/h)
R	COVID-19 reproduction number
T	Exposure time
V	Volume of the building zone (unit:m^3)
α	COVID-19 population prevalence rate
σ	Average CO_2 generation rate by each occupant (unit:m^3/h)
γ	Occupants' inhalation rate (unit:m^3/h)
λ	Virus inactivation rate (unit:1/h)
θ	Damper angle

environment, the ventilation demand can be measured by the viral emission load. The viral emission load can be expressed in terms of the infectious dose emission rate or the quanta emission rate [17]: (a) The 'infectious dose' refers to the quantity of the pathogen. And the infectious dose emission rate is the number of pathogens released by the infector(s) per unit time. The well-known dose-response model [18] adopts the 'infectious dose' for risk assessment of respiratory diseases. (b) The 'quantum' is a hypothetical infectious dose unit, which is defined as the dose of pathogens required to cause infection in 63% of susceptible individuals. The quanta emission rate is the number of quanta generated by the infector(s) per unit time. The quanta emission rate describes the pathogen's infectivity as well as the infectious source strength of the outbreak [17]. The Wells-Riley model [19] uses the 'quanta emission rate' for risk assessment of respiratory diseases. In the existing literatures, several ventilation strategies have been developed to control the COVID-19 infection risk based on the viral emission load. Kurnitski et al. [20] proposed a ventilation design method based on the Wells-Riley model to calculate the required outdoor air ventilation rate to control the COVID-19 infection risk in indoor spaces. The outdoor air ventilation rate can be determined with the quanta emission rate and the given probability of infection. Schibuola et al. [21] proposed a ventilation scheme to limit the COVID-19 contagion in school environment via increasing ventilation rates. Methods proposed in Refs. [20,21] can efficiently determine the proper ventilation rate to control the COVID-19 infection risk. The above methods are designed with the assumption that there is one infectious person in the building zone. However, in the real scenario, it is very likely that there are multiple infectors in the building zone and the number of infectors is changing, especially when the disease prevalence rate in the population is high. In Ref. [22], Wang et al. proposed a DCV strategy based on the occupant density detection algorithm considering both energy efficiency and infection control. This strategy applies YOLO algorithm [23] for occupancy detection based on video frames from surveillance cameras. This strategy can detect the real-time zone occupancy and then determine the possible number of infectors to calculate required ventilation rate. However, this strategy requires camera devices as well as advanced occupancy detection algorithms. The additional hardware cost and privacy concerns may limit its application in many scenarios [24].

The ventilation methods based on viral emission load require the knowledge of the number of infectors, which is usually not available in real-world scenarios. In addition to the viral emission load, the virus quanta concentration [25] can be a more direct indicator of the ventilation demand when controlling indoor infection risk. However, directly detecting and measuring the airborne virus concentration is extremely difficult and slow, and often involves a complicated sample collection process [26,27]. Fortunately, several researches reported that indoor CO_2 can be used as a good proxy for pathogen concentration and infection risk of airborne transmission diseases since CO_2 is co-exhaled with aerosols containing pathogens by infectors. Rudnick et al. [28] derived the relationship between CO_2-based rebreathed fraction and infection risk of airborne transmission diseases. Using this relationship, infection risks of several diseases such as measles, influenza, and rhinovirus were evaluated. Based on Rudnick's work [28], Cammarata et al. [29] developed a new model for estimating infection risk using CO_2 as the indicator, which could consider the sanitization and non-continuous conditions. Peng et al. [30] derived analytical expressions of CO_2-based risk proxies for COVID-19 and applied them to various typical indoor environments. Measurements of indoor CO_2 concentration can be achieved by various low-cost CO_2 sensors [31]. Thus, choosing the indoor CO_2 as the indicator of virus concentration for infection control would be potential and suitable for mass deployment in practice.

Several CO_2-related ventilation strategies have been proposed to control the infection risk of airborne transmission diseases. Zivelonghi et al. [32] developed a natural ventilation strategy to mitigate aerosol infection risk in school buildings based on CO_2 monitoring. Rivas et al. [33] studied the natural ventilation impact on exposure to SARS-CoV-2 in terraces using the indoor CO_2 concentration as the proxy for risk assessment. In Ref. [34], Stabile et al. developed ventilation procedures to minimize the airborne transmission of viruses in classrooms. A novel feedback control strategy using CO_2 concentrations is proposed for naturally-ventilated classrooms. Schibuola et al. [21] proposed a ventilation scheme to limit the COVID-19 contagion in school environments via increasing ventilation rates. The procedure to assess the COVID-19 infection risk in indoor spaces based on CO_2 monitoring is also developed. Zhang et al. [35] proposed an occupancy-aided ventilation strategy using the CO_2-based risk proxy. The optimal occupancy schedule can be determined to minimize the loss of work productivity while satisfying the constraint on infection risk. Gilio et al. [36] conducted a surveillance activity based on real-time CO_2 monitoring to evaluate the effectiveness of some ventilation protocols and suggested tailored corrective actions to limit the infection risk.

The above studies investigated various CO_2-based ventilation strategies to control the infection risk. However, these studies do not involve the design of the demand-controlled ventilation strategy for the infection risk control. Demand-controlled ventilation (DCV) strategy is a smart ventilation strategy which can achieve energy-efficient control of IAQ. Developing CO_2-based DCV strategy in the context of controlling COVID-19 transmission risk would be of great significance for limiting COVID-19 contagion and reducing building energy consumption. Although the idea that CO_2 concentration can be used as the indicator of infection risk has been well studied in the existing literatures, how to design a practical CO_2-based demand-controlled ventilation strategy based on this idea to limit the spread of COVID-19 remains a question. To fill this research gap, this paper designs a novel CO_2-based demand-controlled ventilation strategy to limit the spread of COVID-19 in indoor

environment. Compared with existing studies, the proposed CO_2-based DCV strategy has the following advantages:

1) The proposed strategy is designed based on the demand-controlled scheme. It can flexibly adjust the outdoor ventilation rate according to the actual changing demand, which can achieve energy-efficient control of IAQ to limit the COVID-19 contagion.
2) The proposed strategy is CO_2-based. CO_2 can indicate the pathogen concentration and infection risk regardless of the number of infectors in the building zone. This allows the proposed strategy to be applied to more practical scenarios where there are multiple infectors, and the number of infectors varies with time.
3) The proposed strategy does not require the occupancy detection to estimate the number of infectors. It only requires CO_2 sensors. Since CO_2 sensors are very mature and low-cost, the proposed strategy is suitable for mass deployment in most existing ventilation systems.
4) The proposed strategy incorporates a more conservative consideration for the number of infectors, which can ensure safer control of infection risk.

The main contributions of this study can be summarized as follows:

1) A novel CO_2-based demand-controlled ventilation strategy is proposed to achieve energy-efficient control of infection risk in indoor environment. The proposed method fills the current research gap in how to design a practical CO_2-based DCV strategy to limit the spread of COVID-19 in indoor environment.
2) The quantitative relationship between CO_2 concentration and infection risk is established considering a more conservative estimation of the number of infectors. Based on this relationship, the sufficient condition to ensure the reproduction number less than 1 is derived.
3) A practical control scheme is designed for the ventilation system to ensure the derived sufficient condition can be satisfied.
4) Case studies of different indoor environments have been conducted on an experimental platform of a real ventilation system to verify the effectiveness of the proposed strategy.

The rest of the paper is organized as follows: Section 2 describes the proposed CO_2-based demand-controlled ventilation strategy to limit the spread of COVID-19 in indoor environments. Section 3 firstly introduces the validation testbed and then describes the testing scenarios used in this study. The experimental results and relevant discussions are presented in Section 4 and 5, respectively. Finally, this paper is concluded in Section 6.

2. Methods

2.1. Modeling airborne COVID-19 transmission risk

2.1.1. COVID-19 quanta concentration model with time-varying outdoor air ventilation rate

The quantity "quanta" is a commonly-used measure to quantify the viral load, which is defined as the dose of airborne droplet nuclei required to cause infection in 63% of susceptible occupants. The evolutions of indoor virus quanta concentration over time can be expressed by:

$$\frac{dn(t)}{dt} = -\left(\frac{q(t)}{V} + \lambda + k\right)n(t) + \frac{ER_q \cdot I(t)}{V} \tag{1}$$

where $n(t)$ represents the quanta concentration (unit: quanta/m^3), V is the volume of the room (unit: m^3) $q(t)$ is the outdoor ventilation rate (unit: m^3/h), $I(t)$ is the number of infectors, k is the virus deposition rate onto surfaces (unit: 1/h), λ is the virus inactivation rate (unit: 1/h). Eq. (1) assumes that the supplied outdoor fresh air can be well mixed with the indoor air. Besides, we do not consider using the air cleaner device to remove indoor viral load. ER_q is the average quanta emission rate for each infectious subject (unit: quanta/h). Details about the estimation of ER_q in different indoor environments can be found in Appendix A in the supplementary materials. In practice, the elimination of infectious particles caused by deposition and inactivation is often small compared with removal by ventilation. Thus, coefficients λ and k can be neglected. Then, eq. (1) becomes:

$$V\frac{dn(t)}{dt} = -q(t)n(t) + ER_q \cdot I(t) \tag{2}$$

Neglecting λ and k is a conservative assumption which slightly reduces the total loss rate of the indoor virus in the simulated model. The ventilation rate determined based on eq. (2) will be slightly more than required in the actual system. It should be noted that we consider the time-varying ventilation rate in eq. (2) since $q(t)$ should be dynamically adjusted according to the actual ventilation demand in DCV systems. Most existing studies [30,34,37] considered the **constant** ventilation rate in eq. (2), which is not applicable to DCV systems. Considering time-varying ventilation rate makes eq. (2) a linear time-variant differential equation, which can be solved by the variation of parameters [38]. The details of the solving process for eq. (2) are presented in Appendix B in the supplementary materials. The solution of the eq. (2) is given by:

$$n(t) = \frac{ER_q}{V}\int_0^t e^{\frac{-1}{V}\int_\tau^t q(s)ds} I(\tau)d\tau \tag{3}$$

2.1.2. Airborne infection risk model and acceptable risk levels

The airborne transmission probability of an infectious respiratory disease can be evaluated using the following model [17]:

$$p = 1 - e^{-D} \ (\%) \tag{4}$$

where p is the infection probability of the susceptible person, D is the virus quanta inhaled by the susceptible person exposed to a certain quanta concentration for a certain period T (i.e., the exposure time). D can be calculated by multiplying the integration of $n(t)$ over time with the inhalation rate of the exposed person (denoted by γ, unit: m^3/h):

$$D = \gamma\int_0^T n(t)dt \tag{5}$$

The basic reproduction number R can be used to determine the acceptable infection probability level which can limit COVID-19 transmission in the population [39]. For a given exposure scenario, R is the ratio between the number of new (secondary) infection cases and the number of infectors in the room. $R > 1$ indicates that the disease can spread in the population. When the value of R becomes larger, the disease will spread more quickly. To contain the COVID-19 transmission in the population, the value of R should be less than 1.

The number of new infection cases equals the product of p and the number of susceptible persons N_s in the room. N_s equals $N - I$. Thus, the reproductive number R for a specific scenario can be estimated by:

$$R = \frac{p(N-I)}{I} = \frac{p(1-\alpha)}{\alpha} \tag{6}$$

Considering that R should be less than 1, the acceptable infection risk level is:

$$p < \frac{\alpha}{(1-\alpha)} \tag{7}$$

It should be noted that close contact with the infector will lead to higher risk of exposure to COVID-19 through short-range droplet transmission [40]. This can be overcome by keeping sufficient physical distance. At 1.5 m distance from the infector, the virus concentration will decrease to a constant level depending on emission and removal mechanism [20]. Since this study does not consider short-range droplet

transmission, in practice, the proposed ventilation strategy hereinafter should be applied together with physical distancing measures.

2.1.3. Validation of the COVID-19 transmission risk model using real cases

Several literatures reported the SARS-CoV-2 transmission events happening in real life and the essential data related these events. These real-world transmission events can be used to validate the above COVID-19 transmission risk model and the estimated virus quanta emission data in Appendix A. The details of these real-world events are summarized in Table 1:

The values of γ and ER_q in these events are as follows: the values of γ for these three events are 1.1 m^3/h. The values of for the 1st, 2nd, and 3rd event are 42.1 quanta/h, 42.1 quanta/h, and 195.5 quanta/h, respectively. Estimation details for these parameters can be found in Appendix A.

With the COVID-19 transmission risk model in this study and the above estimated parameters, the number of cases infected by the single index case can be predicted. In the following table, the predicted values are compared with the real number of infections reported.

It can be seen from Table 2 that the predicted number of infected persons is close to the real number of infected persons which demonstrates that the COVID-19 transmission risk model in this study can accurately reflect the real scenario.

2.2. Relationship between the infection risk and the average CO_2 level during the exposure time

In previous works, most assumed that there is only one infector in each building zone [20,21]. However, this is not always the case in real-world scenarios. For instance, when there are more than 50 occupants in the room, with the population prevalence rate α higher than 2%, it is very likely that the number of infectors I in the room is more than one. I is usually estimated as the product of α and N. α is usually estimated according to the daily COVID-19 statistics [45]:

$$\alpha = \frac{N_{new} D_u}{P(1 - f_{un})} \tag{8}$$

where N_{new} is the number of daily new COVID cases, f_{un} is the fraction of unreported COVID cases, P is the population, and D_u is the duration of the infectious period of the COVID-19.

In this study, we consider the latest COVID-19 situation in Singapore. N_{new} is chosen as 2950, which is the average number of daily new cases in Singapore from Apr 19, 2022 to Apr 25, 2022 according to the COVID-19 statistics published by the Ministry of Health, Singapore [46]. Singapore has transitioned into the phase of living with COVID-19 since Aug 2021 and treats COVID-19 as endemic, which could be similar to the scenarios in US. Thus, we choose f_{un} as 75%, which was estimated by the CDC in US (CDC estimates that from Feb 2020 to Sep 2021, 1 in 4.0 (95% UI 3.4–4.7) COVID-19 infections were reported (UI denotes the uncertainty interval) [47]).The population of Singapore is 5.69 million. The duration of the infectious period D is 10 days [48]. Based on the above data, the population prevalence rate α of the COVID-19 considered in this study can be calculated and it equals 2.07%.

Table 1
Details of the real-world COVID-19 transmission events.

Event details	1st event [41]	2nd event [42]	3rd event [43]
Event date	Jan 24, 2020	Feb 20, 2020	Mar 10, 2020
Event location	A restaurant in Guangzhou, China	A meeting room in Germany	A choir rehearsal hall of the Skagit Valley Chorale
Number of primary cases	1	1	1
Number of secondary infected cases during the event	9	≥11	33–53
Number of occupants in total	21	14	61
Volume of the space/m^3	127[a]	189[b]	810
Outdoor ventilation rate/h^{-1}	0.6	0.2[c]	0.35–1.05 [44]
Exposure time/h	1.25	9.5	2.5

[a] The space where the air is recirculated and mixed [44].
[b] The space height is assumed to be 2.7 m.
[c] The space was naturally ventilated with all windows closed during the meeting and the outdoor airflow rate can be assumed as 0.2 h^{-1} which is solely provided by infiltration [44].

It should be noted that the actual number of infectors may not be strictly equal to αN. For example, when $\alpha N = 2.4$, there could be two or three infectors in the room. As for the ventilation design, we prefer more conservative settings to ensure that the indoor pollutants can still be maintained below the threshold value even in the worst case. Therefore, we can assume that the actual number of infectors in the room I equals:

$$I = \lceil \alpha N \rceil \tag{9}$$

where $\lceil \cdot \cdot \rceil$ is the ceiling function. $\lceil x \rceil$ maps x to the least integer greater than or equal to x. It should be noted that eq. (9) is a more conservative consideration of the number of infectors compared to directly using $I = \alpha N$. Using eq. (9) is more suitable for the practical scenario due to the following reasons: First, it would be possible that the actual number of infectors can sometimes exceed αN. If the ventilation scheme is designed assuming $I = \alpha N$, the supplied fresh air may be inadequate during some period, causing the indoor virus concentration higher than the specified threshold. Second, from the probabilistic view, there is little chance that the number of infectors in the room exceeds $\lceil \alpha N \rceil$ for a long time. In most cases, the number of infectors will be less than or equal to $\lceil \alpha N \rceil$. Thus, assuming the number of infectors to be $\lceil \alpha N \rceil$ is conservative enough.

We introduce a new variable, the deviation ratio d, which is defined as the ratio of $\lceil \alpha N \rceil$ to αN. Then, combining eq. (3) and eq. (3), we can obtain:

$$n(t) = \frac{ER_q}{V} \int_0^t e^{\frac{-1}{V}\int_\tau^t q(s)ds} \alpha d(\tau) N(\tau) d\tau \tag{10}$$

Similar to eq. (1), the evolutions of indoor CO_2 level $C(t)$ (unit: ppm) over time can be expressed by:

$$V\frac{dC(t)}{dt} = -q(t)(C(t) - C_{out}) + \sigma N(t) \times 10^6 \tag{11}$$

where C_{out} is the CO_2 concentration in outdoor environment, which approximately equals 400 ppm. σ is the average CO_2 generation rate by each occupant (unit: m^3/h). Details about the estimated values for σ in different indoor environments can be found in Appendix C in the supplementary materials. The solution of eq. (11) is given by:

$$C(t) - C_{out} = \frac{\sigma \times 10^6}{V} \int_0^t e^{\frac{-1}{V}\int_\tau^t q(s)ds} N(\tau) d\tau \tag{12}$$

Since d in eq. (10) is not a constant variable, we cannot directly establish the proportional relationship between $n(t)$ and $C(t) - C_{out}$. Suppose the upper bound of d is $d_{\max}$, then, with the established COVID-19 transmission risk model in Section 2.1 and the CO_2 dynamics model eq. (12), we can derive the following constraint for the indoor CO_2 concentration to ensure the reproduction number is less than 1 to limit the COVID-19 contagion:

$$C_{avg} \le C_{ub} = C_{out} + \frac{\sigma \times 10^6}{\gamma ER_q \alpha d_{\max} T} \ln\left(\frac{1-\alpha}{1-2\alpha}\right) \tag{13}$$

where C_{avg} is the average CO_2 concentration during the exposure period $[0, T]$ (i.e., $C_{avg} = \int_0^T C(t)dt/T$) and C_{ub} is the required CO_2 upper bound. The detailed derivation process for eq. (13) is given in Appendix D. Thus,

Table 2
Comparison results between the real number of infected persons and the predicted number of infected persons by the COVID-19 transmission risk model in this study.

	Predicted infection risk/%	Number of susceptible persons	Predicted number of infected persons	Real number of infected persons
1st event	53.2%	20	11	9
2nd event	100%	13	13	≥11
3rd event	46.9%–85.0%	60	28–51	32–52

the relationship between the infection risk and the average CO_2 level during the exposure time can be established via eq. (13).

To calculate the value of C_{ub}, we should know the value of $d_{\max}$. The following figure shows values of d as a function of N given different prevalence rates:

As shown in Fig. 1, when there are large number of occupants in the room, the value of d is close to 1. The value of d increases significantly when there are less occupants. For instance, when $N < 20$ with $\alpha = 1\%$, the value of d is higher than 4. When the value of αN is close to zero, the value of d tends to be infinite. However, in most cases, the value of d is not that large. Setting a large value for $d_{\max}$ is unnecessary and leads to very low setpoint of CO_2 level. This may result in over-ventilation and waste much energy. According to Fig. 1 and the definition of d, we can know that $d \leq 2$ always holds when $N \geq (2\alpha)^{-1}$. The value of $d_{\max}$ can be set as 2. Then, maintaining the indoor CO_2 level equal to or lower than C_{ub} (calculated by eq. (13), with $d_{\max} = 2$) can ensure $R < 1$ for cases when $N \geq (2\alpha)^{-1}$.

For the cases when $N < (2\alpha)^{-1}$, the value of d is larger than 2. Since the value of αN is less than 0.5, it is most likely that there is no more than one infector in the room. Thus, under these cases, it can be assumed that there is only one infector in the room. According to Ref. [20], the required outdoor ventilation rate per infector q_{pi} for a given infection rate p can be calculated by:

$$q_{pi} = \frac{\gamma E R_q T}{\ln\left(\frac{1}{1-p}\right)} \tag{14}$$

To ensure $R < 1$ (i.e., $p < \alpha/(1-\alpha)$), for the cases when $N < (2\alpha)^{-1}$, the outdoor ventilation rate should be higher than q_{lb}:

$$q_{lb} = \frac{\gamma E R_q T}{\ln\left(\frac{1-\alpha}{1-2\alpha}\right)} \tag{15}$$

The established CO_2-infection risk relationship in this section is similar with those in existing studies such as [28,30]. The main difference between the established one and those in existing studies lies in how to consider and determine the number of infectors in this relationship. The existing studies either assumed the known number of infectors (mostly $I = 1$) [28] or estimate the number of infectors via $I = \alpha N$ [30]. We adopt a more conservative consideration $I = \lceil \alpha N \rceil$ and re-derived the CO_2-infection risk relationship. In the following section, we will derive the sufficient condition to ensure $R < 1$ based on the established relationship in Section 2.2 and then design a novel control scheme for the actual ventilation system.

2.3. Proposed CO_2-based ventilation strategy to mitigate COVID-19 transmission risk

The control rules discussed in Section 2.2 can be recapitulated as the following proposition:

Proposition 1. *When $N \geq (2\alpha)^{-1}$, if **condition A** is satisfied, then $R < 1$; When $N < (2\alpha)^{-1}$, if **condition B** is satisfied, then $R < 1$.*Where:

condition A: the indoor CO_2 level C is maintained equal to or lower than C_{ub} (calculated by eq. (13), with $d_{\max} = 2$),
condition B: the outdoor ventilation rate q is maintained equal to or higher than q_{lb} (calculated by eq. (15)).

It should be noted that condition B also includes the condition that q equals q_{lb}. q_{lb} is the required outdoor ventilation rate for one infector to make the reproduction number R just equal to 1. Maintaining $q = q_{lb}$ can only ensure $R = 1$ (instead of $R < 1$) if there is one infector in the building zone all the time. However, when $N < (2\alpha)^{-1}$ (i.e., $\alpha N < 0.5$), it would be less likely that there is one infector in the building zone all the time from the probabilistic point of view. Thus, maintaining $q = q_{lb}$ can still ensure $R < 1$ when $N < (2\alpha)^{-1}$.

Condition A and condition B are not contradictory. To maintain C below an upper bound, the airflow rate should be kept at a relatively high level. On the other hand, increased outdoor ventilation rate will decrease the indoor CO_2 level. Either the set of condition A is included in the set of condition B, or the set of condition B is included in the set of condition A. Based on this, we can propose a new proposition with a stricter and more conservative condition to ensure $R < 1$:

Proposition 2. *If both **condition A** and **condition B** are satisfied, then $R < 1$.*

"both ***condition A*** and ***condition B*** are satisfied" is the **sufficient condition** to ensure$R < 1$. Proposition 2 combines two circumstances in proposition 1 and does not require knowing the exact number of occupants. It requires that both condition A and condition B should be satisfied all the time regardless of the number of occupants. Based on Proposition 2, we can design the ventilation strategy which does not require occupancy detection.

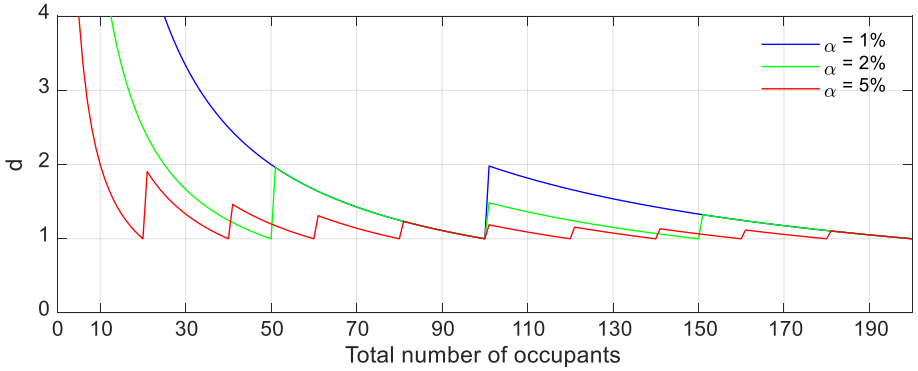

Fig. 1. The values of d ($d = \lceil \alpha N \rceil / \alpha N$) as a function of N, given different prevalence rates α.

Fig. 2 shows the framework of the proposed ventilation strategy. First, the CO_2 upper bound and the airflow lower bound are calculated by the eq. (13) and eq. (15), respectively. Subsequently, these parameters are input to the controller. The controller measures the real-time airflow rate and CO_2 concentration, and compares them with the corresponding bound values. Then, the controller calculates the required change of damper angle and adjusts the damper angle to the expected value, ensuring that both condition A and B can be satisfied. The detailed flowchart of the calculation algorithm in Fig. 2 is shown in Fig. 3. It should be noted that the range of the damper angle is from 0° to 90° (0° corresponds to the fully open state and q reaches the maximum; 90° correspond to the fully closed state and q is 0). The controller keeps monitoring the real-time outdoor ventilation rate and CO_2 concentration and adjusts the damper angle. The monitoring interval in this study is set as 30 s.

To ensure that both condition A and B can be satisfied, we can design the algorithm to control the indoor CO_2 level and the outdoor ventilation rate based on the following schemes:

a) A CO_2-PID control loop is implemented to maintain the indoor CO_2 level C at the C_{ub}. This is to ensure condition A can be satisfied. If $C > C_{ub}$, reduce the damper angle to increase q and vice versa. It should be noted that lower CO_2 setpoint can ensure lower infection rate but lead to higher energy consumption. Maintaining C just at C_{ub} is a good compromise between energy saving and limiting the COVID-19 contagion.

b) In the process of the CO_2-PID control, q is being monitored all the time. As long as q is lower than q_{lb}, deactivate the CO_2-PID control and reduce the damper angle to increase q until $q \geq q_{lb}$. Due to the increase in q, C may be significantly lower than C_{ub}. This is to ensure condition B can be satisfied. When $q \geq q_{lb}$, the CO_2-PID control is activated again.

As for the airflow controller, using a proportional controller is enough to achieve good performance since the adjustment of damper angle will directly affect the airflow rate passing through it (e.g., increasing the damper angle will immediately lead to a decrease in the airflow rate). As for the CO_2 controller, since the CO_2 dynamics have inertia and are more complex, a PID controller is adopted to ensure good control performance. The above schemes are illustrated in Fig. 3.

However, we found that some oscillations may occur if the algorithm is designed only based on the schemes shown in Fig. 3. The oscillation process is illustrated in Fig. 4. As shown in Fig. 4, when $q < q_{lb}$, the CO_2-PID is deactivated, and the damper angle is reduced to increase q until $q \geq q_{lb}$. When q returns to the value higher than q_{lb}, the CO_2-PID is activated. If the indoor CO_2 level is lower than C_{ub}, the CO_2-PID will then

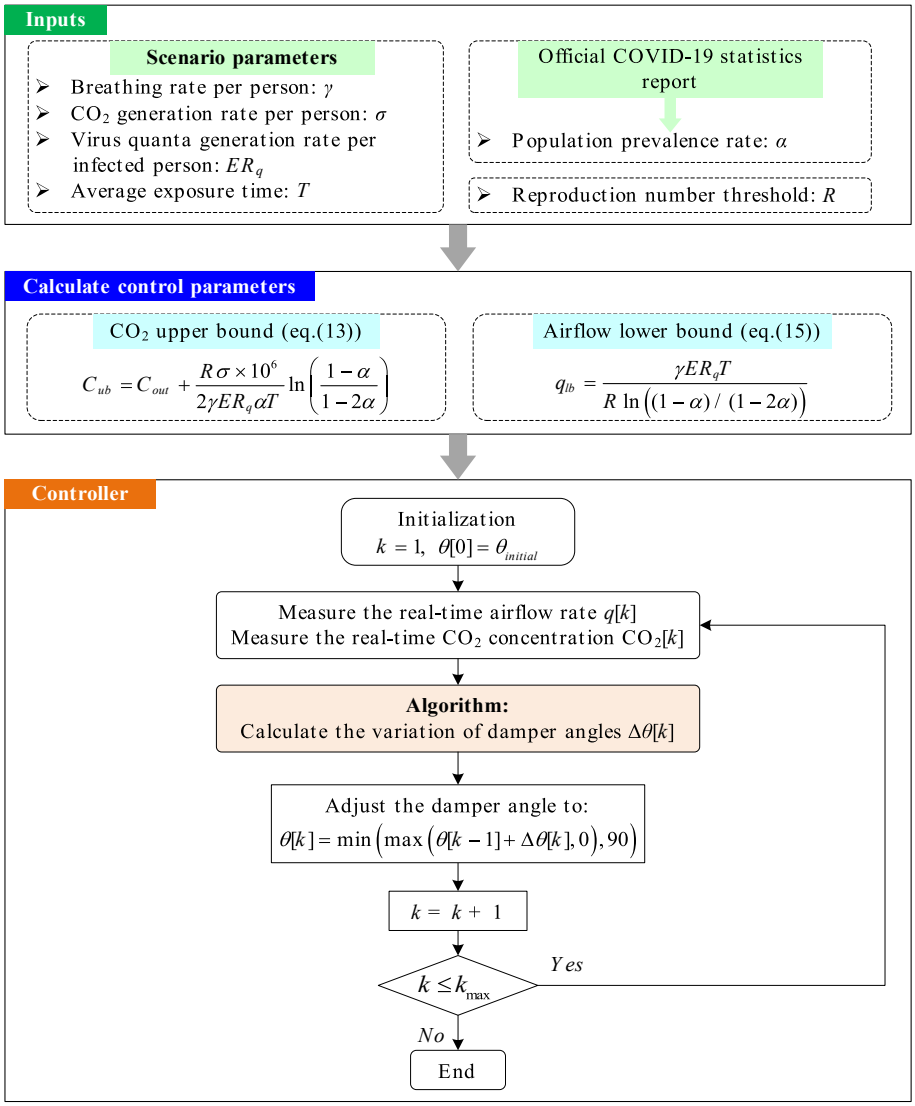

Fig. 2. Basic framework of the proposed ventilation strategy.

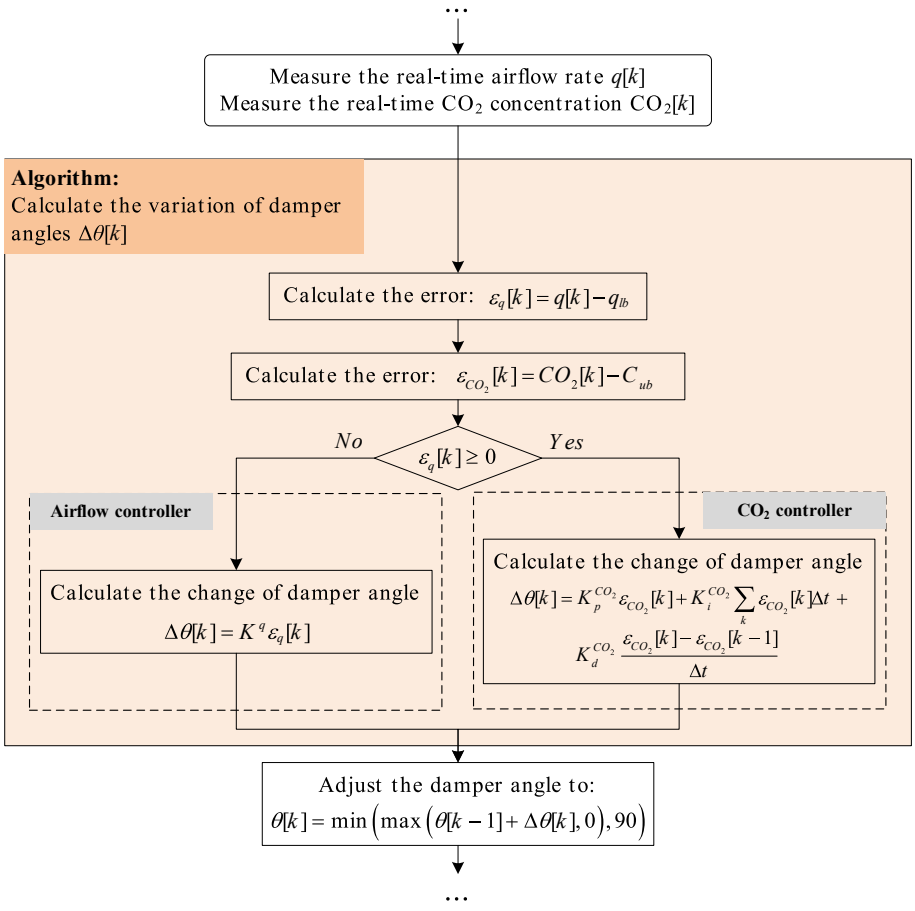

Fig. 3. Control scheme for the ventilation system to ensure both condition A and condition B can be satisfied.

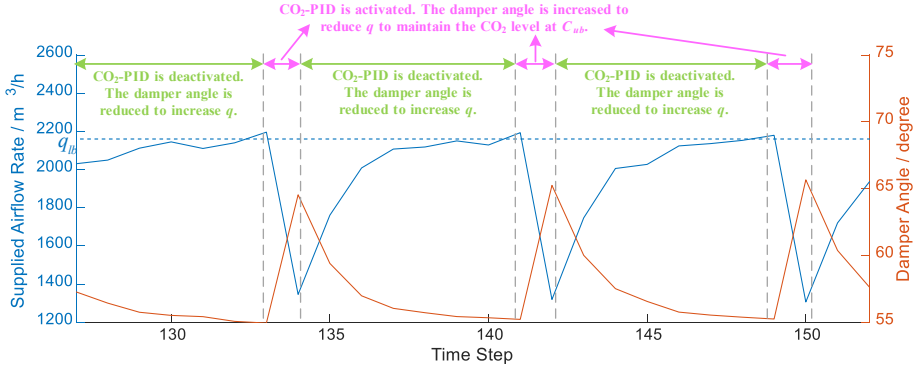

Fig. 4. Illustration of the oscillation process of q and damper angle. The trajectories of q and damper angle are obtained from the experiments in which the control algorithm implemented is based on the schemes shown in Fig. 3.

increase the damper angle to reduce q so that C can be increased and maintained at C_{ub}. This may cause q to fall below q_{lb} again. The above process will repeat, causing significant oscillation of q and damper angle. In addition, as shown in Fig. 4, q will be lower than q_{lb} at most time during the oscillation. This means that condition B cannot be satisfied.

To remedy the above problem, we further improved the control scheme. Fig. 6 shows the improved control scheme for the ventilation system to ensure both condition A and condition B can be satisfied. A new indicator called *flag* is introduced. The initial value of *flag* is 0. When q falls below q_{lb}, $flag = flag + 1$. When C rises above C_{ub}, $flag = 0$.

1) $flag > 0$ means that q falls below q_{lb} and C has remained below C_{ub} after q falls below q_{lb}. In this stage, if the CO_2-PID is activated to maintain the indoor CO_2 level at C_{ub}, q has to be reduced to increase the CO_2 level back to C_{ub}, and the value of q may be lower than q_{lb}. Thus, the CO_2-PID should not be activated during this stage and the damper angle should be adjusted according to the change of q (i.e., adjust the damper angle to maintain the q at q_{lb}).
2) $flag = 0$ means that C starts to rise above C_{ub} and maintaining $q = q_{lb}$ is not enough to ensure $C < C_{ub}$. Thus, the CO_2-PID should be activated again. And the damper angle should be adjusted according to the change of CO_2 (i.e., adjust the damper angle to maintain $C = C_{ub}$).

With the above improvements, the oscillations can be eliminated and the value of q can be kept above q_{lb}. In Fig. 5, the trajectory of q obtained in the experiment using the improved control scheme (shown in Fig. 6) is compared with that using the original control scheme (shown in Fig. 3). We can see from Fig. 5 that the improved control algorithm can efficiently solve the problem of oscillation.

3. Experimental setup

3.1. Validation testbed

We set up a validation testbed (shown in Fig. 7) which consists of an experimental system connected to a virtual building zone to verify the effectiveness of the proposed ventilation strategy. The experimental ventilation system includes a variable speed centrifugal fan, a duct network, duct terminals and dampers. The supply fan pumps the air, and the duct network distributes the air flow into different terminals. In this study, only one terminal is used. The damper with a control board is installed in each terminal to control the supplied airflow. The control board has an STM32F103 microcontroller which uses the Cortex-M3 core with a maximum CPU speed of 72 MHz. The control algorithm for the ventilation system (illustrated in Fig. 6) is implemented by the microcontroller to calculate the desired change of damper angle. The damper can rotate from 0° (corresponding the fully open state) to 90° (corresponding the fully closed state) driven by a servo motor with an angular resolution of ±0.18°. Additionally, the supply fan is also equipped with a similar control board which has an STM32F103 microcontroller. This microcontroller implements the PID control algorithm to keep the fan pressure at the fixed setpoint. The averaging pitot tube (APT) [49] is adopted in this study to measure the airflow rate in each terminal. The APT is installed in each damper and its measurement error is within 0.6%.

The IAQ dynamics in the virtual building zone are simulated in Matlab. The control board in the terminal needs to read the real-time CO_2 concentration value from the simulated indoor environment in Matlab. In our validation testbed, the control board interfaces with the host computer (where the Matlab software is installed) via the Modbus protocol. The simulation model of the SARS-CoV-2 quanta concentration variation is given by eq. (16), which is the discrete version of eq. (2)

$$n[k+1]-n[k]=-\frac{q[k]n[k]}{V}\Delta t+\frac{ER_q\cdot I[k]}{V}\Delta t \tag{16}$$

where Δt is the simulation step size and it is set as 10 s in this study. $q[k]$ is the airflow measured in the real ventilation system. Similarly, the simulation model of the CO_2 concentration variation is given by:

$$C[k+1]-C[k]=\frac{q[k]}{V}(C_{out}-C[k])\Delta t+\frac{\sigma N[k]}{V}\Delta t \tag{17}$$

$I[k]$ equals $\lceil \alpha N[k] \rceil$ according to eq. (9). $N[k]$ is determined according to the given occupancy profile in the corresponding scenario.

Fig. 8 shows the experiment framework of the proposed ventilation strategy. In each control step, the ventilation control strategy obtains the real-time values of CO_2 and airflow and calculates the adjustment angle of the damper. Then the servo motor adjusts the damper angle to the calculated value. The variation of n during the experiment is recorded. After the experiment, the records of n are used to assess the infection risk of the testing scenarios.

3.2. Description of the testing scenarios

In this study, we consider three typical indoor environments as the testing scenarios: library, restaurant, and gymnasium. Details about these testing scenarios can be found in Table 3:

The values of breathing rate γ are retrieved from the literature [20]. Details about the estimation of ER_q and σ can be found in Appendix A and C in the supplementary material.

Fig. 9 shows the simulated occupancy profile for each testing scenario. The profiles are generated to imitate the occupancy patterns in real building scenarios. First, the profile includes high occupancy periods and low occupancy periods. Second, the profile contains some random fluctuations due to the uncertainty in real scenarios. The time range for each testing scenario is from 7:00 to 21:00. In the simulation, the number of infectors is determined according to the occupancy profile (using eq. (9)).

This study assumes CO_2 generation rate for each occupant is constant for each scenario, which implies that the metabolic rate for each occupant is also constant. However, for the building scenario like gyms and stadiums, occupants' metabolic rates are usually higher than other scenarios and may fluctuate significantly, depending on the level of activities occupants take part in. Assuming a constant CO_2 generation rate may reduce the control accuracy of the proposed strategy in these scenarios.

The study in Ref. [50] provides a novel metabolic rate prediction modeling method, in which a computer vision algorithm is designed to monitor occupants' activities based on the videos acquired from the camera. A neural network is established to predict the occupant's metabolic rate. As for gyms and alike building scenarios, this metabolic rate prediction method [50] can be integrated into the proposed strategy to overcome the problem of fluctuating metabolic rates. It is expected that integration of the metabolic rate prediction into our proposed strategy could improve its ventilation control performance in gyms and alike building scenarios.

If there is no camera installed or the information from surveillance cameras is not available, the information of occupants' activities for different time periods may be obtained from the activity/class schedules for the gym/stadium. Then, the average occupants' metabolic rate for each activity can be obtained from Ref. [51] in which the metabolic rates for various kinds of physical activities are provided. CO_2 generation rates for different time periods can be calculated using eq. (7) in Ref. [50] with the obtained metabolic rates. Finally, the required CO_2 upper bound values for different time periods can be calculated

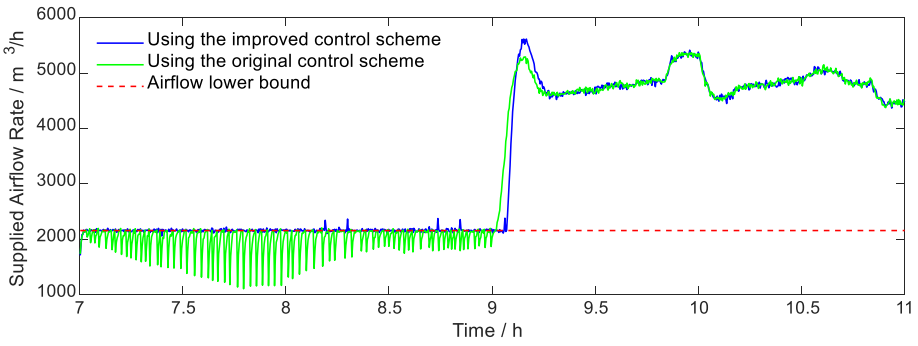

Fig. 5. Trajectories of q obtained in the experiment. The simulated scenario is the library (details can be found in Section 3).

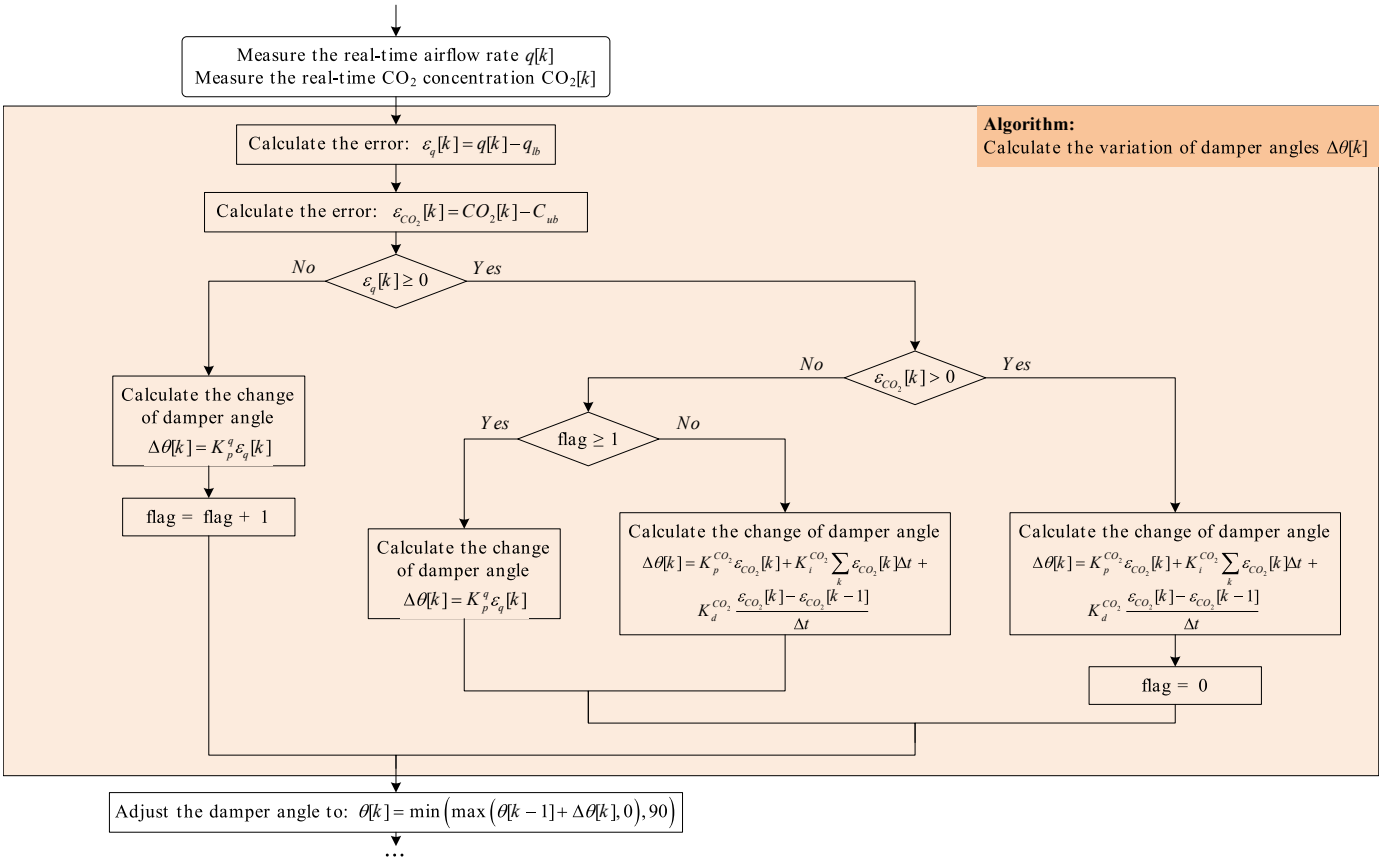

Fig. 6. Improved control scheme for the ventilation system to ensure both condition A and condition B can be satisfied.

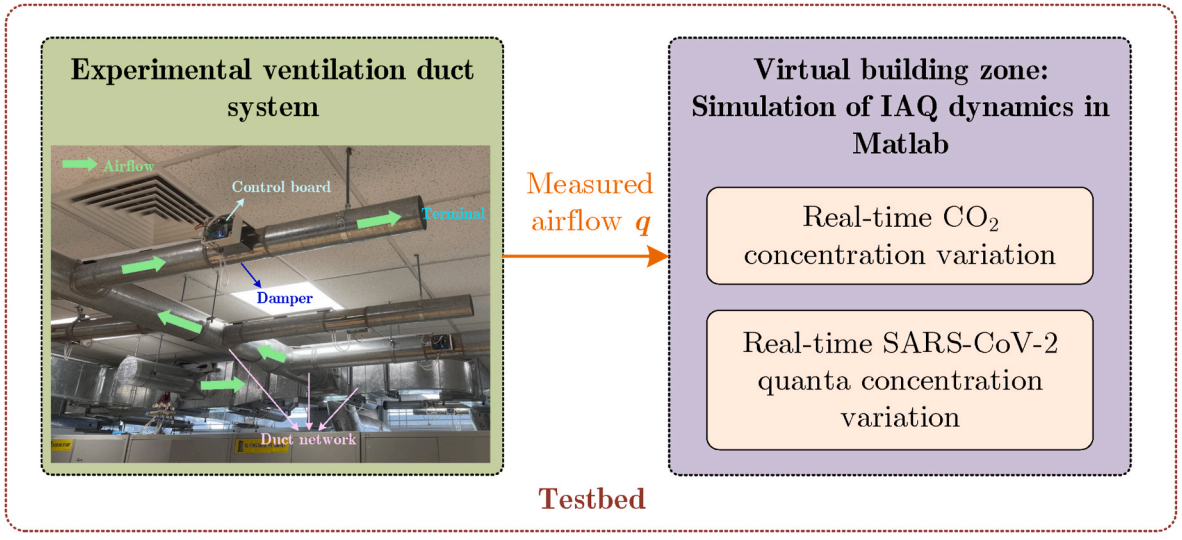

Fig. 7. Schematic of the validation testbed. The testbed includes an experimental ventilation system connected to a virtual building zone. In the virtual building zone, IAQ dynamics are simulated in Matlab. It should be noted that the airflow used in the simulation is the airflow measured in the real ventilation system.

according to eq. (13).

4. Results

4.1. Infection control performance of the proposed ventilation strategy

The proposed ventilation strategy is tested under three different scenarios: library, restaurant, and gym. Details of testing scenarios can be found in Table 3. The R threshold is set as 1. Testing results under these three scenarios are plotted in Figs. 10 and 11. Results of time evolution of airflow and CO_2 concentration are shown in Fig. 10. Results of time evolution of virus quanta concentration n, infection rate p and R-value are shown in Fig. 11. In Fig. 10, the curve in blue (i.e., time evolution of airflow) is the measured curve (measured from the experimental ventilation system) while the curve in red (i.e., time evolution of CO_2 concentration) is the simulated curve (simulated via the IAQ

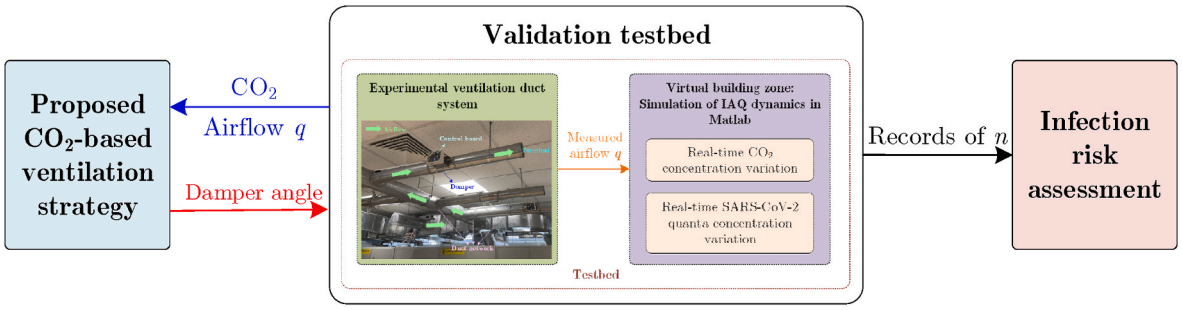

Fig. 8. Experiment framework of the proposed CO_2-based ventilation strategy. n denotes the SARS-CoV-2 quanta concentration.

Table 3
Description of the testing scenarios used in this study.

Scenario	Area/m^2	Height/m	Maximum Occupancy	T[a]/h	γ/m^3•h^{-1}	σ/m^3•h^{-1}	ER_q/quanta•h^{-1}
Library	300	3	100	8	0.54	0.0173	10.2
Restaurant	350	3	150	1	1.1	0.0248	42.1
Gymnasium	500	3	100	1	3.3	0.05	19.2

[a] T: Occupants' exposure time in the given scenario.

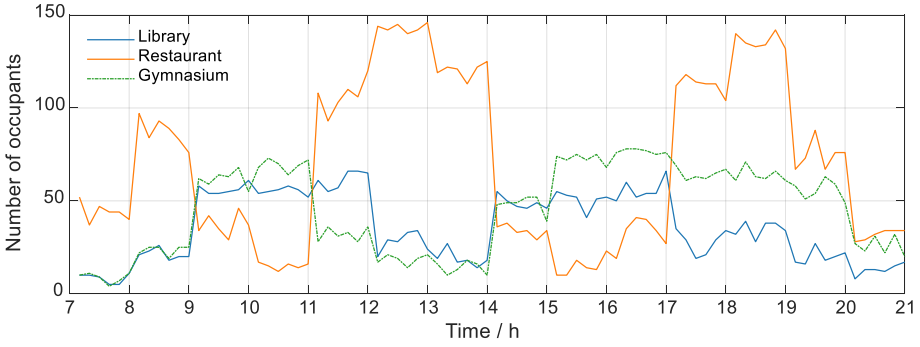

Fig. 9. Occupancy profiles for the testing scenarios.

dynamics model based on the measured airflow). In Fig. 11, all curves are the simulated curves (simulated via the IAQ dynamics model based on the measured airflow).

The infection rate is calculated according to the eq. (4) and eq. (5):

$$p = 1 - e^{-\gamma \int_t^{t+T} n(t)dt} \quad (\%) \tag{18}$$

The R-value is calculated according to eq. (7), using the infection rate p and prevalence rate α. The prevalence rate α is 2.07% (details about the calculation of α are presented in Section 2.3). It should be noted that p is calculated based on the integration of n over a certain time period (i.e., the exposure time T). For example, in the library scenario ($T = 8$ h), the value of p at 18:00 is calculated based on the integration of n from 10:00 to 18:00; the value of p at 9:00 is calculated based on the integration of n from 7:00 to 9:00 (the occupants start to be present in the zone from 7:00).

It can be seen from Fig. 10 that the proposed strategy can satisfy both condition A and B in each testing scenario. That is, the indoor CO_2 concentration can be maintained lower than or equal to the required CO_2 upper bound while the airflow can be maintained higher than or equal to the required airflow lower limit. For example, in the library scenario, the airflow rate is maintained at the lower limit (2160 m^3/h) from 7:00 to 9:00. During this period, the CO_2-PID is deactivated, and the indoor CO_2 concentration is lower than the upper bound (600 ppm). Since 9:00, the number of occupants increases. The CO_2 concentration starts to increase and exceeds the upper bound. This activates the CO_2-PID to maintain the CO_2 concentration at the upper bound. As shown in Fig. 10 (a), the airflow significantly increases from 9:00. The CO_2 concentration slightly exceeds the upper bound for several minutes and then quickly falls back to the upper bound. At 12:00, the number of occupants drops obviously, leading to the reduction in CO_2 generation. To maintain the CO_2 concentration at the upper bound, the CO_2-PID increases the damper angle to reduce the airflow rate until the airflow rate falls below the lower limit. Then, the CO_2-PID is deactivated, and the damper angle is adjusted to maintain the airflow rate at the lower bound. The following process is similar and not be described again.

From Fig. 10, we can also find that the trend of the airflow trajectory is similar to the trend of the occupancy profile. The airflow rate is increased during high occupancy periods and vice versa, which means that the proposed strategy can efficiently adjust the ventilation according to the actual demand.

As shown in Fig. 11, the trajectory of the R-value in each scenario is below the threshold (i.e., less than 1). The highest R-value which occurs in these three scenarios (library, restaurant, and gym) is 0.744, 0.860, and 0.859, respectively. This demonstrates that the proposed ventilation strategy can efficiently control the infection risk and limit the disease contagion.

The following table compares airflow requirements between the proposed strategy and the EN16798–1:2019 standard [52] in which the airflow rate is calculated according to the occupancy and space area.

Table 4 shows that the required airflow rate of the proposed strategy is higher than that of existing standards. Thus, when applying the proposed strategy to the actual systems which are designed according to existing standards like EN16798–1:2019, the airflow rate required to

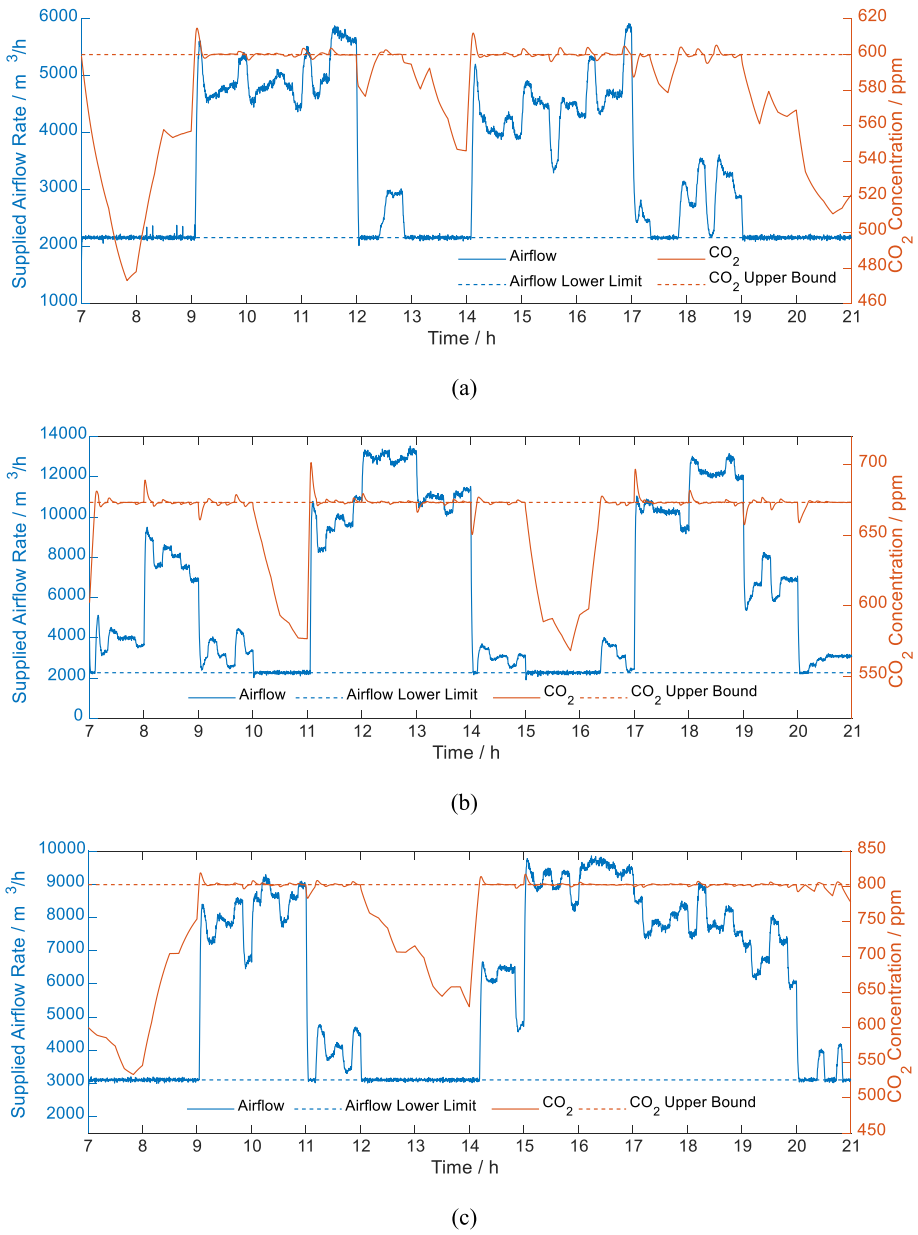

Fig. 10. Time evolution of the airflow and CO_2 concentration in different scenarios: (a) library, (b) restaurant, (c) gym. The corresponding airflow lower limit (library: 2160 m^3/h, restaurant: 2269 m^3/h, gym: 3105 m^3/h) and the CO_2 upper bound (library: 600 ppm, restaurant: 673 ppm, gym: 803 ppm) are also shown.

implement the proposed strategy may not be achieved due to the capacity limit of these systems. Under these circumstances, the proposed strategy should be implemented together with several safe management measures, such as, reducing the maximum occupancy, reducing occupants' exposure time, compulsory to wear masks indoors, etc. These measures can help to further reduce occupants' infection risk.

4.2. Evaluation of energy saving potential of the proposed ventilation strategy

In this section, energy consumption of the proposed strategy is compared with that of the fixed ventilation control (abbreviated as FVC hereafter) strategy. Under the FVC scheme, the outdoor ventilation rate is fixed regardless of the number of occupants. Generally, the ventilation rate of the FVC strategy is designed based on zone maximum occupancy. Similar to this principle, in this study, the number of infectors $I_{\max}$ when the occupancy reaches maximum is estimated according to eq. (9). Then, the required ventilation rate for the FVC is calculated by multiplying $I_{\max}$ with the required outdoor ventilation rate per infector (eq. (15)).

The power consumption of the ventilation system can be calculated by eq. (20) [53].:

$$E = \frac{q(h_{out} - h_{in})}{COP} + E_d\left(\frac{q}{q_d}\right)^2 \tag{19}$$

In eq. (19, the first term is the power consumed by the chiller system while the second term is the power consumed by the fan system. q is the outdoor ventilation rate. h_{out} denotes the specific enthalpy of the outdoor air and h_{in} denotes the indoor specific enthalpy. COP is the coefficient of performance, and it is assumed to be 2.5 [53]. In this study, h_{in} is assumed to be 48.7 kJ/kg which corresponds to the indoor temperature of 24 °C and the indoor relative humidity of 50%. h_{out} is assumed to be 79.3 kJ/kg which corresponds to the outdoor temperature of 28 °C (the mean annual temperature of Singapore) and the outdoor relative humidity of 84% (the mean annual relative humidity of Singapore). q_d is the design ventilation rate, which is assumed to be 1.2 times of the required ventilation rate for the FVC scheme. E_d is the power

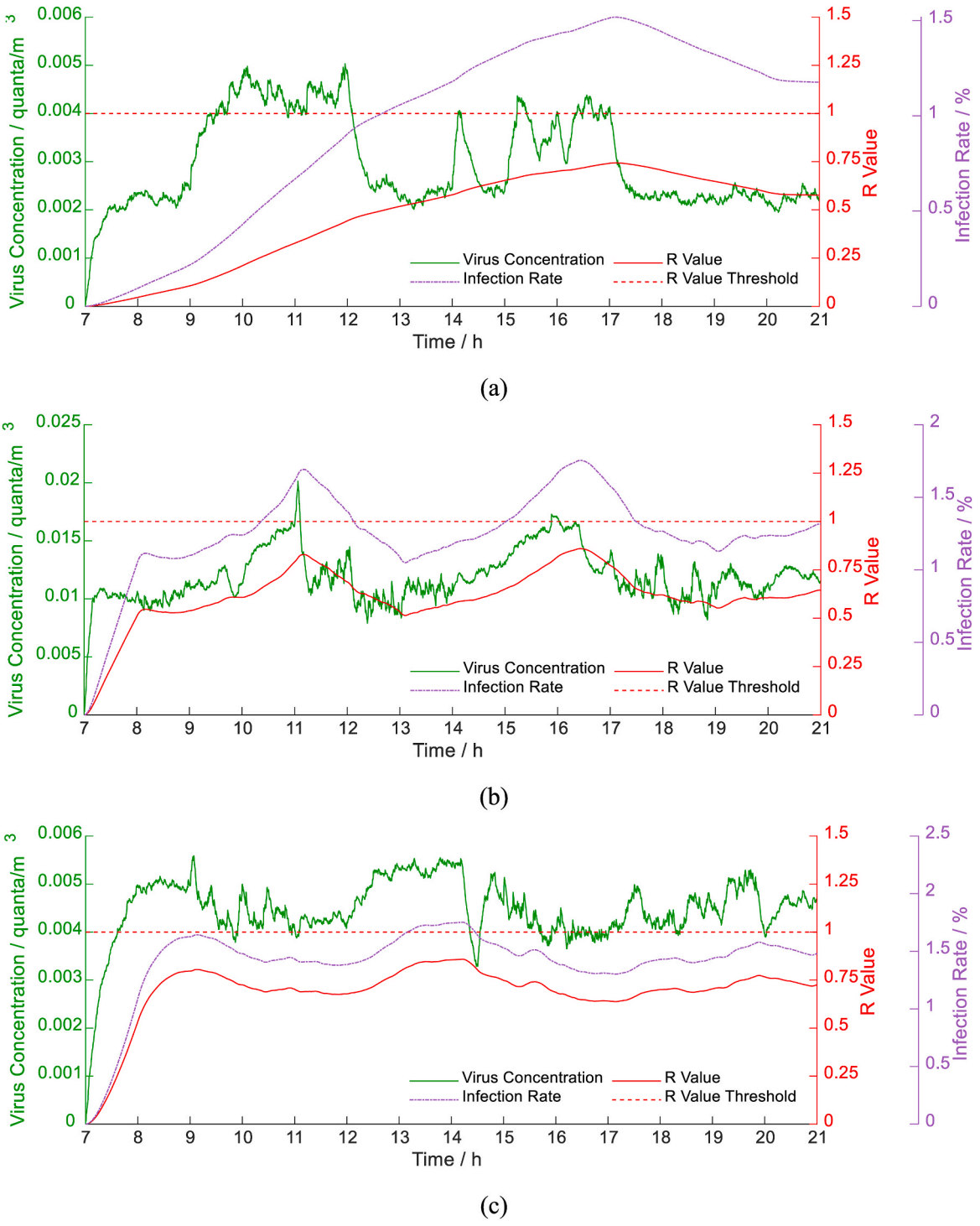

Fig. 11. Time evolution of the virus quanta concentration, infection rate, and R-value in different scenarios: (a) library, (b) restaurant, (c) gym. The R-value threshold is also shown.

consumption of the fan system when the ventilation rate reaches q_d. In different indoor environments, the required ventilation rate is different and thus the scale of the fan system will be different. The values of E_d in this study are estimated according to the datasheets on an official website [54] of a manufacturer of industrial fan products. The values of q_d in the studied indoor environments (library, restaurant, and gymnasium) are 7800 m^3/h, 11000 m^3/h and 11000 m^3/h, respectively. And the values of E_d for these indoor environments are 11 kW, 15 kW and 15 kW, respectively.

We can calculate the energy consumption by integrating the power consumption (eq. (19)) over the simulated time period (i.e., 7:00–21:00). Results of the energy consumption of the proposed ventilation strategy and the FVC strategy are shown in Fig. 12:

As shown in Fig. 12, the proposed ventilation strategy can significantly reduce energy consumption compared with the FVC strategy. Specifically, in the studied indoor environments (library, restaurant and gymnasium), the proposed strategy can save 53.2%, 28.9% and 40.1% of the energy compared with the FVC strategy, respectively. This demonstrates that the proposed ventilation strategy can achieve energy-efficient control of IAQ to limit COVID-19 contagion.

Table 4
Airflow rate per person (unit: m^3/h) under the proposed strategy and the EN16798–1:2019 standard when the number of occupants reaches 70% of the design (maximum) number of occupants.

Scenario	Proposed ventilation strategy	EN16798–1:2019 standard [52]		
		Category I	Category II	Category III
Library	84.6	57.6	40.3	23.0
Restaurant	90.0	52.8	37.0	21.1
Gym	123.7	72	50.4	28.8

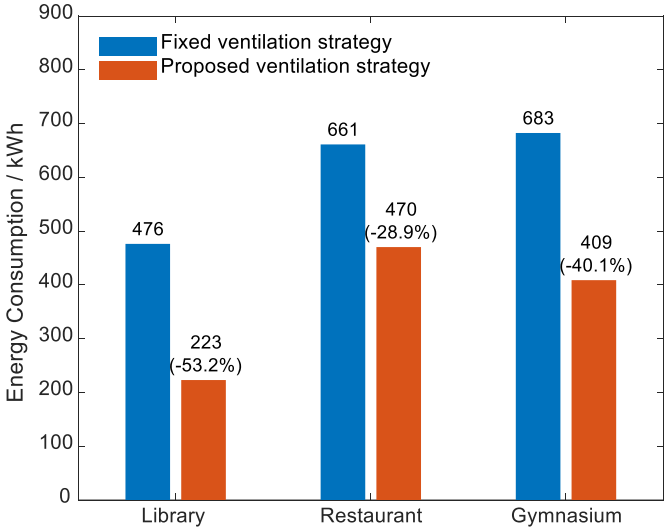

Fig. 12. Energy consumption of the proposed ventilation strategy and the fixed ventilation strategy during the simulated time period (7:00–21:00). The energy saving potential of the proposed strategy compared with the fixed ventilation strategy is also marked in the figure.

We also calculated energy consumption of the conventional occupancy-based DCV strategy (abbreviated as O-DCV) that enforces minimum required airflow rate q_{lb} (calculated by eq. (15)) for each infector. Under the O-DCV strategy, the number of infectors I at different times is assumed to be known and the airflow rate q is calculated as $q = I \times q_{lb}$. Table 5 compares energy consumption between the O-DCV strategy and the proposed CO_2-based DCV strategy:

Table 5 shows that energy consumption of the O-DCV is 15%–30% lower than that of the proposed strategy. This is because O-DCV assumes I is known and the airflow rate is accurately determined according to I, i.e., the supplied airflow is just enough for diluting infectious pathogens emitted by infectors. However, the proposed strategy assumes I is unknown and adjusts the airflow according to measured CO_2, which adopts the conservative estimation for I. The supplied airflow for the proposed strategy may be slightly more than required, causing more energy consumption compared to O-DCV. This slight over-ventilation can provide safer guarantee for $R < 1$ to limit COVID-19 contagion.

Table 5
Energy consumption of the proposed strategy and the O-DCV strategy during simulation time period (unit: kWh).

	Proposed CO_2-based DCV	Conventional O-DCV
Library	223	190
Restaurant	470	324
Gym	409	311

5. Discussions

When applying the proposed DCV strategy in actual ventilation systems, several important practical issues should be considered. In this section, we firstly elaborate engineering application potentials of the proposed DCV strategy and then present detailed discussions on several practical issues relevant to this strategy, such as CO_2 measurement problems, occupants' thermal comfort, impact on overall system design, as well as limitations of the proposed strategy. In addition, we also provide possible solutions to some of these issues.

5.1. Engineering application potentials

COVID-19 puts considerable pressure on health systems and societies. It would be of significance to develop practical and efficient ventilation strategies to limit COVID-19 transmission in indoor environments. This study proposes a novel CO_2-based demand-controlled ventilation strategy in the context of controlling COVID-19 infection risk. The proposed strategy can efficiently maintain the reproduction number less than 1 while saving 30–50% of energy compared with the fixed ventilation scheme. The proposed strategy only requires CO_2 sensors and does not require occupancy detection sensors, which makes it suitable for mass deployment in most existing ventilation systems. Additionally, the proposed strategy is CO_2-based. CO_2 can indicate pathogen concentration and infection risk regardless of the number of infectors in the space. This allows the proposed strategy to be applied to more practical scenarios where there are multiple infectors, and the number of infectors varies with time.

5.2. CO_2 measurement

The CO_2 measurement will be very important for the proposed method. This study adopted the well-mixed assumption for CO_2. However, in actual building zones, indoor CO_2 concentration is unevenly distributed. The non-uniformity of the CO_2 distribution will be more obvious in the larger building zones. Under these scenarios, the uneven CO_2 distribution as well as its diffusion and mixing mechanics may result in the time delay and loss of accuracy for the CO_2 measurement. For this study, several strategies could be adopted to mitigate the adverse effects of uneven CO_2 on the CO_2 measurement. According to Ref. [55], considering the scenario with only one CO_2 sensor installed, we suggest that the CO_2 sensor can be installed at the exhaust duct [55]. indicates that the relative error between the CO_2 concentration measured in the exhaust duct compared with the average CO_2 concentration within the breathing zone is less than 5% under the mixing ventilation scenario, which can meet the requirements of sensor accuracy in several standards [56,57].

The results in Fig. 6 in Ref. [55] also show that the curves of transient trends of the CO_2 measured in the exhaust duct and the average CO_2 within the zone almost coincide with each other, which means that CO_2 measurement delay is small and can be neglected for the building zone with relatively small size. However, for the large building zone, although the CO_2 concentration measured at the exhaust duct can reflect the average CO_2 concentration in the building zone, the measurement delay due to the air mixing process would become obvious and cannot be neglected. For these scenarios, to mitigate the measurement delay problem, we could install multiple CO_2 sensors at different points in the building zone and use the average value of these sensors. Several studies have already adopted this method to ensure the accurate monitoring of indoor CO_2 concentration [58,59].

5.3. Thermal comfort

In addition to controlling infection risk, occupants' thermal comfort cannot be neglected when designing actual ventilation systems. The DCV strategy in this paper is proposed for the dedicated outdoor air

system (DOAS) to deliver proper outdoor fresh air to dilute virus-laden respiratory particles for limiting COVID-19 transmission as well as maintaining good IAQ. Generally, the DOAS can handle most latent loads as well as part of sensible loads for the building zone: the outdoor fresh air is dehumidified in the air handling unit and then delivered to each building zone; sensible cooling is the byproduct of the dehumidification process, which can meet a portion of sensible loads. A parallel terminal system (such as the fan-coil unit, the active thermosiphon beam (ATB) terminal unit [60]), which is independent of the DOAS, is required to handle the other portion of sensible loads (mostly) and latent loads [61]. In practice, the DOAS, controlled by the ventilation strategy proposed in this paper, should operate with the ATB terminal unit to limit the COVID-19 transmission while ensuring occupants' thermal comfort.

Additionally, the selection and placement of the supply air outlets of the DOAS should be carefully considered in the actual design to ensure the fresh air is delivered without introducing unacceptable noise or causing the sensation of a draft on the occupant. For instance, the outlet size should be determined according to the required ventilation rate for each building scenario to ensure the supply air velocity is in the suitable range (i.e., 3–5 m/s [62,63]).

5.4. Impact on the system design

The proposed strategy is a novel ventilation strategy to limit COVID-19 contagion in indoor environments, which may be different from existing ventilation strategies in some respects. Impact of this strategy on the overall system design needs to be considered. These impacts and possible modifications/retrofits to existing systems are discussed in this subsection.

First, in the context of controlling COVID-19 transmission risk, more outdoor air needs to be conditioned before delivered to the space. From results in Table 4, we can know that the outdoor ventilation rate is higher than that required for IAQ control in conventional systems. Due to the capacity limit, especially during extreme weather periods (e.g., very hot and humid weather in Singapore), more sensible/latent loads need to be handled and the DOAS may only handle limited parts of these loads. Under these circumstances, the capacity limit of the DOAS may be compensated by increasing the capacity of the parallel terminal system which is independent of the DOAS. For instance, the space could equip with more ATB terminal units [60] to provide more capacity for handling additional sensible/latent loads.

Second, the ventilation demand estimated in this study may lead to overdesign problem at the system level. This is mainly due to the overestimation of the number of infectors I in the space. In this study, we adopted a conservative consideration for I, i.e., $I = \lceil \alpha N \rceil$. When the proposed strategy is applied to the ventilation system connected to single large zone which has relatively large design number of occupants (such as restaurants, where there could be multiple infectors), the overestimation problem is not obvious. However, when applied to the system connected to several small zones (e.g., 10-person office rooms, where there could be only one or zero (mostly) infector according to community prevalence rate), the proposed strategy assumes at least one infector is present, which may cause overdesign problems. Under these scenarios, the airflow lower limit q_{lb} can be further reduced by multiplying a reduction factor $\lambda (\lambda < 1)$. $\lambda = \alpha N_{design}^{(i)}$ if $\alpha N_{design}^{(i)} < 1$ ($N_{design}^{(i)}$ is the design (maximum) number of occupants for the ith room). Multiplying q_{lb} by $\lambda = \alpha N_{design}^{(i)}$ implies the assumption that there is at least λ infector ($\lambda < 1$) in this room, instead of one infector. This assumption is reasonable from the probablistic view: when the number of occcupants reaches $N_{design}^{(i)}$, the expected value for the number of infectors present in the room during a period is $\alpha N_{design}^{(i)}$. Given this, since infection risk is evaluated by the integration of n during exposure period, this assumption can ensure $R < 1$ for the exposure period.

5.5. Limitations of the proposed strategy

This paper focuses on designing a CO_2-based demand-controlled ventilation scheme in the context of limiting COVID-19 contagion. However, there are several limitations:

First, the proposed strategy is designed based on the well-mixed assumption for CO_2 and infectious pathogens, which means they are evenly distributed in the space. However, in large building zones, CO_2 and infectious pathogens are usually unevenly distributed. For our study, the uneven CO_2 distribution as well as its diffusion and mixing mechanics may result in the time delay and loss of accuracy for the CO_2 measurement. Detailed discussion about CO_2 measurement problems and possible solutions are presented in Section 5.2.

Second, one of the inputs of the proposed strategy is the prevalence rate of COVID-19. However, this parameter is highly uncertain in real-world scenarios: It needs to know the number of infections in population, but large portion of infections are not reported, especially those who are asymptomatic. Researchers, including CDC, have conducted several studies [47,64–66] on the prediction for unreported ratio using epidemiological models, to better reflect the full burden of COVID-19. To adapt the current study to general use, the unreported ratio used to calculate the prevalence rate should be updated according to the latest report from the CDC/the department of health or the latest related studies, which could reflect the current epidemiological scenario more accurately. In addition, the ratio of unreported cases can be also estimated based on the test positivity rate using a simple nowcasting model [67]. This nowcasting model is developed specially for the epidemiological scenarios in US. Modifications may be required when applying this model to other regions.

Third, when estimating the quanta emission rate, this study assumes that the viral load in sputum (denoted by v_L) is constant. However, v_L (unit: RNA copies/mL) can vary by several orders of magnitude depending on the stage of the disease and the individual [68]. [69] pointed out that the relationship between CO_2 concentration and the number concentration of released droplets could be established with reasonable uncertainty but the relationship between CO_2 concentration and RNA concentration is more complicated and may include much uncertainty due to large variability in viral loads. In this study, we adopted a conservative assumption, i.e., chose a relatively high value for the viral load $v_L = 10^9$ which may cause higher ventilation rate to dilute pathogens.

6. Conclusions

This paper presents a novel CO_2-based DCV strategy in the context of controlling COVID-19 transmission in indoor environments. Case studies of different indoor environments have been conducted on an experimental platform of a real ventilation duct system to verify the effectiveness of the proposed strategy. Results show that the proposed strategy can efficiently maintain $R < 1$ to limit COVID-19 contagion while saving about 30%–50% of energy compared with the fixed ventilation scheme. In future studies, we intend to incorporate more practical factors into the ventilation control framework: 1) To overcome CO_2 measurement problems (i.e., loss of accuracy, measurement delay) caused by the uneven CO_2 distribution in large building zones, we aim to design the CO_2-based DCV strategy which considers uneven spatial distribution of the CO_2 and indoor pollutants, to maintain good IAQ and limit the spread of COVID-19 in large building zones. 2) Since ventilation control from the aspect of limiting COVID-19 transmission is different from the conventional control scheme, problems regarding the impact on overall system design should be further studied. For instance, proper estimation methods of the number of infectors should be proposed for different scenarios, which should ensure the DCV strategy designed based on these estimations can achieve efficient infection control while not causing severe overdesign problems.

CRediT authorship contribution statement

Bingxu Li: Writing – original draft, Visualization, Validation, Software, Methodology, Investigation, Formal analysis, Data curation, Conceptualization. **Wenjian Cai:** Writing – review & editing, Resources, Project administration, Funding acquisition.

Declaration of competing interest

The authors declare that they have no known competing financial interests or personal relationships that could have appeared to influence the work reported in this paper.

Acknowledgements

This work was supported by the Building and Construction Authority under Grant BCA 94.23.1.3., Singapore.

Appendix. Supplementary data

Supplementary data to this article can be found online at https://doi.org/10.1016/j.buildenv.2022.109232.

References

[1] Coronaviridae Study Group of the International Committee on Taxonomy of Viruses, The species Severe acute respiratory syndrome-related coronavirus: classifying 2019-nCoV and naming it SARS-CoV-2, Nat. microb. 5 (4) (2020) 536–544.
[2] WHO, WHO coronavirus (COVID-19) dashboard, Available: https://covid19.who.int/, 2022.
[3] WHO, Classification of omicron (B.1.1.529): SARS-CoV-2 variant of concern, Available: https://www.who.int/news/item/26-11-2021-classification-of-omicron-(b.1.1.529)-sars-cov-2-variant-of-concern, 2021.
[4] C. Del Rio, S.B. Omer, P.N. Malani, Winter of omicron-the evolving COVID-19 pandemic, JAMA 327 (4) (2022) 319–320.
[5] W. Yang, J. Shaman, SARS-CoV-2 Transmission Dynamics in South Africa and Epidemiological Characteristics of the Omicron Variant, medRxiv, 2021.
[6] K. Ito, C. Piantham, H. Nishiura, Relative instantaneous reproduction number of Omicron SARS-CoV-2 variant with respect to the Delta variant in Denmark, J. Med. Virol. 94 (2022) 2265–2268.
[7] R. Wang, J. Chen, G.-W. Wei, Mechanisms of SARS-CoV-2 evolution revealing vaccine-resistant mutations in Europe and America, J. Phys. Chem. Lett. 12 (49) (2021) 11850–11857.
[8] J. Chen, R. Wang, N.B. Gilby, G.-W. Wei, Omicron variant (B. 1.1. 529): infectivity, vaccine breakthrough, and antibody resistance, J. Chem. Inf. Model. 62 (2) (2022) 412–422.
[9] M. Hoffmann, et al., The Omicron variant is highly resistant against antibody-mediated neutralization–implications for control of the COVID-19 pandemic, Cell 185 (3) (2022) 447–456.
[10] C.J. Murray, COVID-19 will continue but the end of the pandemic is near, Lancet 399 (10323) (2022) 417–419.
[11] M. Scudellari, How the pandemic might play out in 2021 and beyond, Nature (2020) 22–25.
[12] WHO, Transmission of SARS-CoV-2: implications for infection prevention precautions: scientific brief, 09 July 2020, Available: https://apps.who.int/iris/bitstream/handle/10665/333114/WHO-2019-nCoV-Sci_Brief-Transmission_modes-2020.3-eng.pdf?sequence=1&isAllowed=y, 2020.
[13] L. Morawska, et al., How can airborne transmission of COVID-19 indoors be minimised? Environ. Int. 142 (2020), 105832.
[14] W.J. Fisk, A.T. De Almeida, Sensor-based demand-controlled ventilation: a review, Energy Build. 29 (1) (1998) 35–45.
[15] Z. Sun, S. Wang, Z. Ma, In-situ implementation and validation of a CO2-based adaptive demand-controlled ventilation strategy in a multi-zone office building, Build. Environ. 46 (1) (2011) 124–133.
[16] C. Zhuang, K. Shan, S. Wang, Coordinated demand-controlled ventilation strategy for energy-efficient operation in multi-zone cleanroom air-conditioning systems, Build. Environ. 191 (2021), 107588.
[17] G.N. Sze To, C.Y.H. Chao, Review and comparison between the Wells-Riley and dose-response approaches to risk assessment of infectious respiratory diseases, Indoor Air 20 (1) (2010) 2–16.
[18] T. Armstrong, C.N. Haas, A quantitative microbial risk assessment model for Legionnaires' disease: animal model selection and dose-response modeling, Risk Anal.: Int. J. 27 (6) (2007) 1581–1596.
[19] E. Riley, G. Murphy, R. Riley, Airborne spread of measles in a suburban elementary school, Am. J. Epidemiol. 107 (5) (1978) 421–432.
[20] J. Kurnitski, et al., Respiratory infection risk-based ventilation design method, Build. Environ. 206 (2021), 108387.
[21] L. Schibuola, C. Tambani, High energy efficiency ventilation to limit COVID-19 contagion in school environments, Energy Build. 240 (2021), 110882.
[22] J. Wang, J. Huang, Z. Feng, S.-J. Cao, F. Haghighat, Occupant-density-detection based energy efficient ventilation system: prevention of infection transmission, Energy Build. 240 (2021), 110883.
[23] J. Redmon, S. Divvala, R. Girshick, A. Farhadi, You only look once: unified, real-time object detection, in: Proceedings of the IEEE Conference on Computer Vision and Pattern Recognition, 2016, pp. 779–788.
[24] S. Wolf, D. Calì, J. Krogstie, H. Madsen, Carbon dioxide-based occupancy estimation using stochastic differential equations, Appl. Energy 236 (2019) 32–41.
[25] M. Conte, et al., Airborne Concentrations of SARS-CoV-2 in Indoor Community Environments in Italy, Environmental Science and Pollution Research, 2021, pp. 1–12.
[26] J. Bhardwaj, S. Hong, J. Jang, C.-H. Han, J. Lee, J. Jang, Recent advancements in the measurement of pathogenic airborne viruses, J. Hazard Mater. 420 (2021), 126574.
[27] H. Yun, J. Yang, J.-H. Seo, J.-R. Sohn, Methodology for sampling and detection of airborne coronavirus including SARS-CoV-2, Indoor Built Environ. 31 (5) (2022) 1234–1241.
[28] S. Rudnick, D. Milton, Risk of indoor airborne infection transmission estimated from carbon dioxide concentration, Indoor Air 13 (3) (2003) 237–245.
[29] A. Cammarata, G. Cammarata, Dynamic assessment of the risk of airborne viral infection, Indoor Air 31 (6) (2021) 1759–1775.
[30] Z. Peng, J.L. Jimenez, Exhaled CO2 as a COVID-19 infection risk proxy for different indoor environments and activities, Environ. Sci. Technol. Lett. 8 (5) (2021) 392–397.
[31] L. Spinelle, M. Gerboles, M.G. Villani, M. Aleixandre, F. Bonavitacola, Field calibration of a cluster of low-cost commercially available sensors for air quality monitoring. Part B: NO, CO and CO2, Sensor. Actuator. B Chem. 238 (2017) 706–715.
[32] A. Zivelonghi, M. Lai, Mitigating aerosol infection risk in school buildings: the role of natural ventilation, volume, occupancy and CO2 monitoring, Build. Environ. 204 (2021), 108139.
[33] E. Rivas, J.L. Santiago, F. Martín, A. Martilli, Impact of natural ventilation on exposure to SARS-CoV 2 in indoor/semi-indoor terraces using CO2 concentrations as a proxy, J. Build. Eng. 46 (2022), 103725.
[34] L. Stabile, A. Pacitto, A. Mikszewski, L. Morawska, G. Buonanno, Ventilation procedures to minimize the airborne transmission of viruses in classrooms, Build. Environ. 202 (2021), 108042.
[35] S. Zhang, Z. Ai, Z. Lin, Occupancy-aided ventilation for both airborne infection risk control and work productivity, Build. Environ. 188 (2021), 107506.
[36] A. Di Gilio, et al., CO2 concentration monitoring inside educational buildings as a strategic tool to reduce the risk of Sars-CoV-2 airborne transmission, Environ. Res. 202 (2021), 111560.
[37] G. Buonanno, L. Stabile, L. Morawska, Estimation of airborne viral emission: quanta emission rate of SARS-CoV-2 for infection risk assessment, Environ. Int. 141 (2020), 105794.
[38] T. Meurer, Analysis and control of linear time-varying systems, Available: https://www.control.tf.uni-kiel.de/en/teaching/summer-term/nonlinear-control-systems/fileadmin/ncs_ss20_chap2.
[39] J.M. Carcione, J.E. Santos, C. Bagaini, J. Ba, A simulation of a COVID-19 epidemic based on a deterministic SEIR model, Front. Public Health (2020) 230.
[40] S. Dhawan, P. Biswas, Aerosol dynamics model for estimating the risk from short-range airborne transmission and inhalation of expiratory droplets of SARS-CoV-2, Environ. Sci. Technol. 55 (13) (2021) 8987–8999.
[41] Y. Li, et al., Probable airborne transmission of SARS-CoV-2 in a poorly ventilated restaurant, Build. Environ. 196 (2021), 107788.
[42] D. Hijnen, et al., SARS-CoV-2 transmission from presymptomatic meeting attendee, Germany, Emerg. Infect. Dis. 26 (8) (2020) 1935.
[43] S.L. Miller, et al., Transmission of SARS-CoV-2 by inhalation of respiratory aerosol in the Skagit Valley Chorale superspreading event, Indoor Air 31 (2) (2021) 314–323.
[44] B. Jones, P. Sharpe, C. Iddon, E.A. Hathway, C.J. Noakes, S. Fitzgerald, Modelling uncertainty in the relative risk of exposure to the SARS-CoV-2 virus by airborne aerosol transmission in well mixed indoor air, Build. Environ. 191 (2021), 107617.
[45] D. Hou, A. Katal, L.L. Wang, Bayesian Calibration of Using CO2 Sensors to Assess Ventilation Conditions and Associated COVID-19 Airborne Aerosol Transmission Risk in Schools, medRxiv, 2021.
[46] Available: https://www.moh.gov.sg/covid-19/statistics.
[47] CDC, Estimated COVID-19 burden, Available: https://www.cdc.gov/coronavirus/2019-ncov/cases-updates/burden.html#whycdcestimates, 2021.
[48] Z. Hu, et al., Clinical characteristics of 24 asymptomatic infections with COVID-19 screened among close contacts in Nanjing, China, Sci. China Life Sci. 63 (5) (2020) 706–711.
[49] C. Cui, W. Cai, H. Chen, Airflow measurements using averaging Pitot tube under restricted conditions, Build. Environ. 139 (2018) 17–26.
[50] J. Wang, J. Huang, Q. Fu, E. Gao, J. Chen, Metabolism-based ventilation monitoring and control method for COVID-19 risk mitigation in gymnasiums and alike places, Sustain. Cities Soc. 80 (2022), 103719.
[51] Compendium of physical activities [Online]. Available: https://download.lww.com/wolterskluwer_vitalstream_com/PermaLink/MSS/A/MSS_43_8_2011_06_13_AINSWORTH_202093_SDC1.pdf, 2011.
[52] E. 16798-1, Energy performance of buildings—ventilation for buildings—Part 1: indoor environmental input parameters for design and assessment of energy performance of buildings addressing indoor air quality, thermal environment,

lighting and acoustics—module M1-6, in: European Committee for Standardization Brussels, Belgium, 2019.
[53] W. Li, S. Wang, A multi-agent based distributed approach for optimal control of multi-zone ventilation systems considering indoor air quality and energy use, Appl. Energy 275 (2020), 115371.
[54] Available: https://fans-uk.aircontrolindustries.com/, 2022.
[55] G. Pei, D. Rim, S. Schiavon, M. Vannucci, Effect of sensor position on the performance of CO2-based demand controlled ventilation, Energy Build. 202 (2019), 109358.
[56] A. Standard, Standard Test Method for Determining Air Change in a Single Zone by Means of a Tracer Gas Dilution, 2011.
[57] CEC, "Building Energy Efficiency Standards for Residential and Nonresidential Buildings," California Energy Commission2019.
[58] S. Cui, M. Cohen, P. Stabat, D. Marchio, CO2 tracer gas concentration decay method for measuring air change rate, Build. Environ. 84 (2015) 162–169.
[59] A. Franco, F. Leccese, Measurement of CO2 concentration for occupancy estimation in educational buildings with energy efficiency purposes, J. Build. Eng. 32 (2020), 101714.
[60] K. Ji, W. Cai, B. Wu, X. Ou, Mechanical design and performance evaluation of active thermosiphon beam terminal units, Build. Environ. 153 (2019) 241–252.
[61] S.A. Mumma, Designing dedicated outdoor air systems, ASHRAE J. 43 (5) (2001) 28–32.
[62] A. Burdick, Advanced Strategy Guideline: Air Distribution Basics and Duct Design, National Renewable Energy Lab.(NREL), Golden, CO (United States), 2011.
[63] A. Bhatia, HVAC-how to size and design ducts, PDH online Course (2001) 22–25. M06-032.
[64] J.P. Ansah, et al., The effectiveness of public health interventions against COVID-19: lessons from the Singapore experience, PLoS One 16 (3) (2021), e0248742.
[65] Z. Peng, et al., Estimating unreported COVID-19 cases with a time-varying SIR regression model, Int. J. Environ. Res. Publ. Health 18 (3) (2021) 1090.
[66] Z. Liu, P. Magal, G. Webb, Predicting the number of reported and unreported cases for the COVID-19 epidemics in China, South Korea, Italy, France, Germany and United Kingdom, J. Theor. Biol. 509 (2021), 110501.
[67] Y. Gu, Estimating true infections revisited: a simple nowcasting model to estimate prevalent cases in the US, Available: https://covid19-projections.com/estimating-true-infections-revisited/, 2020.
[68] Y. Pan, D. Zhang, P. Yang, L.L. Poon, Q. Wang, Viral load of SARS-CoV-2 in clinical samples, Lancet Infect. Dis. 20 (4) (2020) 411–412.
[69] N. Kappelt, H.S. Russell, S. Kwiatkowski, A. Afshari, M.S. Johnson, Correlation of respiratory aerosols and metabolic carbon dioxide, Sustainability 13 (21) (2021) 12203.